PNAS PLUS

Catalogue of abrupt shifts in Intergovernmental Panel on Climate Change climate models

Sybren Drijfhout[a,b,1], Sebastian Bathiany[c,d], Claudie Beaulieu[b], Victor Brovkin[d], Martin Claussen[d,e], Chris Huntingford[f], Marten Scheffer[c], Giovanni Sgubin[g], and Didier Swingedouw[h]

[a]Research and Development, Weather and Climate Modeling, Royal Netherlands Meteorological Institute, 3730AE De Bilt, The Netherlands; [b]National Oceanography Centre Southampton, University of Southampton, Southampton SO14 3ZH, United Kingdom; [c]Department of Environmental Sciences, Wageningen University, 6708PB Wageningen, The Netherlands; [d]The Land in the Earth System, Max Planck Institute for Meteorology, 20146 Hamburg, Germany; [e]Center for Earth System Research and Sustainability, Universität Hamburg, 20146 Hamburg, Germany; [f]Climate System Group, Centre for Ecology and Hydrology, Wallingford OX10 8BB, United Kingdom; [g]Laboratoire des Sciences du Climat et de l'Environnnement, Institut Pierre Simon Laplace, 91191 Gif-sur-Yvette, Paris, France; and [h]Environnements et Paleoenvironnements Oceaniques et Continentaux, University of Bordeaux, 33615 Pessac, France

Edited by Mark H. Thiemens, University of California, San Diego, La Jolla, CA, and approved September 11, 2015 (received for review June 11, 2015)

Abrupt transitions of regional climate in response to the gradual rise in atmospheric greenhouse gas concentrations are notoriously difficult to foresee. However, such events could be particularly challenging in view of the capacity required for society and ecosystems to adapt to them. We present, to our knowledge, the first systematic screening of the massive climate model ensemble informing the recent Intergovernmental Panel on Climate Change report, and reveal evidence of 37 forced regional abrupt changes in the ocean, sea ice, snow cover, permafrost, and terrestrial biosphere that arise after a certain global temperature increase. Eighteen out of 37 events occur for global warming levels of less than 2°, a threshold sometimes presented as a safe limit. Although most models predict one or more such events, any specific occurrence typically appears in only a few models. We find no compelling evidence for a general relation between the overall number of abrupt shifts and the level of global warming. However, we do note that abrupt changes in ocean circulation occur more often for moderate warming (less than 2°), whereas over land they occur more often for warming larger than 2°. Using a basic proportion test, however, we find that the number of abrupt shifts identified in Representative Concentration Pathway (RCP) 8.5 scenarios is significantly larger than in other scenarios of lower radiative forcing. This suggests the potential for a gradual trend of destabilization of the climate with respect to such shifts, due to increasing global mean temperature change.

abrupt climate change | critical transitions | CMIP5 | IPCC | climate change

The gradual rise in greenhouse gas concentrations is projected to drive a mostly smooth increase in global temperature (1). However, the Earth system is suspected to have a range of "tipping elements" with the characteristic that their gradual change will be punctuated by critical transitions on regional scales (2, 3). That is, for relatively small changes in atmospheric concentrations of greenhouse gases, parts of the Earth system exhibit major changes. The recent fifth Assessment Report (AR5) of the Intergovernmental Panel on Climate Change (IPCC) presents a catalog of possible abrupt or irreversible changes (table 12.4 in ref. 4). This catalog builds on a previous literature review (2) of components believed to have the potential for an acceleration of change as fossil fuel burning changes atmospheric composition and thus radiative forcing.

The expert elicitation (2) motivated discussion of a multitude of environmental threats to the planet in which it was critically argued that atmospheric carbon dioxide concentration should not cross 350 ppm (5), trying to determine what constitutes safe levels of global warming. This threshold was suggested in ref. 5 to minimize the risk due to massive sea ice change, sea level rise, or major changes to terrestrial ecosystems and crops. An alternative purely temperature-based threshold is that from the Copenhagen accord, setting an upper limit of 2° (6). However, major uncertainty exists in knowledge of climate sensitivity (7), which makes it difficult to relate this warming level to a precise CO_2 concentration. However, despite this and the growing interest in the societal effects of such transitions, there has been no systematic study of the potential for abrupt shifts in state-of-the-art Earth System Models.

To explore what may be deduced from the current generation of climate models in this context, we analyze the simulations produced by Coupled Model Intercomparison Project 5 (CMIP5) (8) that were used to inform the IPCC. CMIP5 provides a compilation of coordinated climate model experiments. Each of 37 analyzed models includes representations of the oceans, atmosphere, land surface, and cryosphere. The climate models have been forced with future changes in atmospheric gas concentrations, depicted in four Representative Concentration Pathways (RCPs) (9), starting in year 2006. Of these, we analyze RCP2.6, RCP4.5, and RCP8.5 to explore a range of changes in radiative forcing, reaching levels of 2.6 $W{\cdot}m^{-2}$, 4.5 $W{\cdot}m^{-2}$, and 8.5 $W{\cdot}m^{-2}$, respectively, by year 2100 (including all available simulations that go beyond 2100). We also analyze historical simulations, capturing changes from preindustrial conditions in year 1850 to the present, and preindustrial control simulations.

To assess future risks of abrupt, potentially irreversible, changes in important climate phenomena, we first need to define what we mean by "abrupt." This term clearly refers to time scale and is usually defined as when changes observed are faster than the time

Significance

One of the most concerning consequences of human-induced increases in atmospheric greenhouse gas concentrations is the potential for rapid regional transitions in the climate system. Yet, despite much public awareness of how "tipping points" may be crossed, little information is available as to exactly what may be expected in the coming centuries. We assess all Earth System Models underpinning the recent 5th Intergovernmental Panel on Climate Change report and systematically search for evidence of abrupt changes. We do find abrupt changes in sea ice, oceanic flows, land ice, and terrestrial ecosystem response, although with little consistency among the models. A particularly large number is projected for warming levels below 2°. We discuss mechanisms and include methods to objectively classify abrupt climate change.

Author contributions: S.D. designed research; S.D., S.B., V.B., G.S., and D.S. performed research; S.D., S.B., C.B., V.B., M.C., C.H., M.S., G.S., and D.S. analyzed data; and S.D., S.B., C.B., V.B., M.C., C.H., M.S., G.S., and D.S. wrote the paper.

The authors declare no conflict of interest.

This article is a PNAS Direct Submission.

Data deposition: All data are freely downloadable from cmip-pcmdi.llnl.gov/cmip5/data_portal.html.

[1]To whom correspondence should be addressed: Email: S.S.Drijfhout@soton.ac.uk.

This article contains supporting information online at www.pnas.org/lookup/suppl/doi:10.1073/pnas.1511451112/-/DCSupplemental.

scale of the external forcing. Here we choose a methodology consisting of three stages. Firstly, we systematically screen the CMIP5 multimodel ensemble of simulations for evidence of abrupt changes using search criteria (*Methods*) to make a first filtering of regions of potentially relevant abrupt events from this dataset (stage 1). These criteria are motivated by the definition of the assessment report, AR5 (4): "A large-scale change in the climate system that takes place over a few decades or less, persists (or is anticipated to persist) for at least a few decades, and causes substantial disruptions in human and natural systems." Other definitions have emphasized the timescales of the change, e.g., 30 y (10), and rapidity in comparison with the forcing (11), which also meet our search criteria. Global maps of quantities with potential to change abruptly are expressed as (*i*) the mean difference between end and beginning of a simulation, (*ii*) the SD of the detrended time series, and (*iii*) the maximum absolute change within 10 y. These maps are made for all scenario runs and compared with values for the preindustrial control runs. When at least two indicators suggest locations of major change, we construct time series for area averages of at least 0.5×10^6 km^2 (roughly 10 by 10 degrees) and visually inspect these for abrupt shifts standing out from the internal variability (stage 2). Subsequently, we check whether the selected cases can indeed be considered examples of abrupt change applying formal classification criteria (*Methods*) such as the criterion that the change should be larger than 4 times the SD of the preindustrial simulation, in combination with additional statistical tests (stage 3).

We find a broad range of transitions passing our classification criteria (Fig. 1, Table 1, and *SI Appendix*, Table S1), which can be grouped into four categories (Table 1 and Fig. 2). They include abrupt shifts in sea ice and ocean circulation patterns as well as abrupt shifts in vegetation and the terrestrial cryosphere. Fig. 2 shows a selected example for each category. All other time series are displayed in Fig. 3. Information on the regions where the shifts occur and the results of the statistical tests used for classification are displayed in *SI Appendix*, Tables S2 and S3, respectively. A list of the climate models and their acronyms is provided in *SI Appendix*, Table S1.

Results

Category I, Type 1, Cases a, b, c, and d: Unforced Bimodal Switches in Sea Ice Cover. Sea ice abrupt changes are particularly common in climate simulations and may be explained by a relatively simple feedback between sea ice and open-ocean convection (12). In preindustrial climate, some models already simulate irregular switches between two regimes as a feature of internal variability (Fig. 2*A*). In four preindustrial cases, they meet the criteria for abrupt shifts, occurring as a sequence of abrupt reversals. In all four cases, these abrupt switches continue throughout the historical period and RCP scenarios, but often become weaker when the climate warms. These switches only appear in the Southern Ocean and mainly coincide with the regions of open-ocean convection, which are the main deep water formation regions in the models (13). During periods when convection brings warm water to the surface, no permanent ice cover can form, allowing cooling of surface water and favoring convection. In addition, the large formation rate of brine during freezing in areas of seasonal sea ice cover destabilizes the water column further, inhibiting the formation of sea ice. On the other hand, once the surface is covered by perennial sea ice, much less brine formation occurs, making the water column more stable, enabling the formation of more sea ice. Accordingly, open-ocean convection occurs mostly in regions featuring seasonal ice cover and seasonal ice-free conditions in the models (13). The dependence of sea ice cover on deep water formation also explains the long residence times of the sea ice regimes between decades and centuries, a feature which is hard to either verify or falsify given the lack of long-term observations.

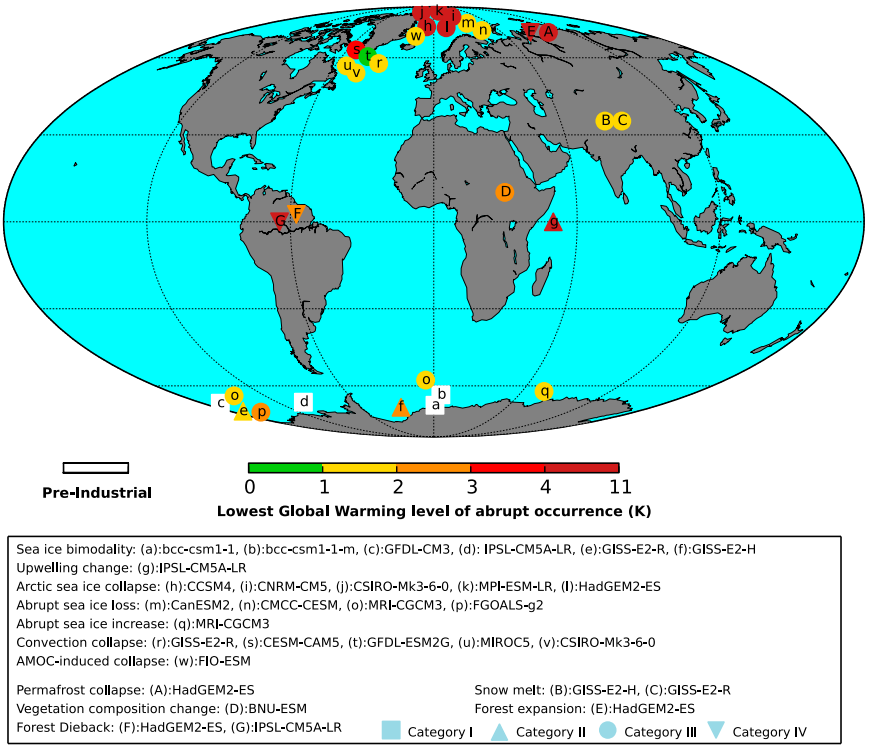

Fig. 1. Geographical location of the abrupt climate change occurrences. All 30 model cases listed in Table 1 are depicted. Of the 41 abrupt shifts, when regarding similar events for different simulations by the same climate model, this reduces to 30 distinct model cases. Marker color indicates the lowest global warming level, at which the abrupt change occurs, and the shape indicates category.

Table 1. Categories of abrupt changes in the CMIP5 model ensemble

Category	Type	Region	Models and scenarios
I (switch)	1. sea ice bimodality	Southern Ocean	BCC-CSM1-1 (all), BCC-CSM1-1-m (all), IPSL-CM5A-LR (all), GFDL-CM3 (all)
II (forced transition to switch)	2. sea ice bimodality	Southern Ocean	GISS-E2-H (rcp45), GISS-E2-R (rcp45, rcp85)
	3. abrupt change in productivity	Indian Ocean off East Africa	IPSL-CM5A-LR (rcp85)
III (rapid change to new state)	4. winter sea ice collapse	Arctic Ocean	MPI-ESM-LR (rcp85), CSIRO-MK3-6-0 (rcp85), CNRM-CM5 (rcp85), CCSM4 (rcp85), HadGEM2-ES (rcp8.5)
	5. abrupt sea ice decrease	regions of high-latitude oceans	CanESM2 (rcp85), CMCC-CESM (rcp85), FGOALS-G2 (rcp85), MRI-CGCM3 (all rcp)
	6. abrupt increase in sea ice	region in Southern Ocean	MRI-CGCM3 (rcp45)
	7. local collapse of convection	Labrador Sea, North Atlantic	GISS-E2-R (all rcp), GFDL-ESM2G (his), CESM1-CAM (rcp85), MIROC5 (rcp26), CSIRO-MK3-6-0 (rcp26)
	8. total collapse of convection	North Atlantic	FIO-ESM (all rcp)
	9. permafrost collapse	Arctic	HADGEM2-ES (rcp85)
	10. abrupt snow melt	Tibetan Plateau	GISS-E2-H (rcp45, rcp85), GISS-E2-R (rcp45, rcp85)
	11. abrupt change in vegetation	Eastern Sahel	BNU-ESM (all rcp)
IV (gradual change to new state)	12. boreal forest expansion	Arctic	HadGEM2-ES (rcp85)
	13. forest dieback	Amazon	HadGEM2-ES (rcp85), IPSL-CM5A-LR (rcp85)

Four categories are listed by type (column 2), region (column 3), and climate model and scenario (column 4). Fig. 2 provides examples of abrupt shifts for each category.

Although open-ocean convection has only been observed once in the present-day Southern Ocean (14), the underlying process possibly played a more important role in preindustrial climate (15). At present, open-ocean convection occurs only in the Mediterranean, Labrador, and Greenland Seas (16). In the Southern Ocean, bottom water formation is observed on continental shelves, through the action of katabatic winds, a small-scale feature not well represented in the present generation of climate models, which instead produce Antarctic bottom water through open-ocean convection (13). However, there is an ongoing debate in the literature as to whether open-ocean convection was indeed a common process in the Weddell Sea in preindustrial times (14, 15). The hypothesis that this can occur is supported by hydrographic data (15) and satellite observations of the Weddell polynia (17), strongly suggesting that open-ocean convection did occur in the Weddell Sea for a few successive years.

Category II, Type 2, Cases e and f: Forced Bimodal Switches in Sea Ice Cover. Bimodal switches in sea ice cover can also be triggered by climate change, which happens in different realizations and two versions of the GISS model (Fig. 2*B*). Feedbacks are similar to those for type 1. In the GISS models, the switches are absent in the preindustrial and historical runs and only appear after a change in climate has occurred. They persist after that moment as a (perpetual) sequence of abrupt shifts. At present, we cannot determine whether these abrupt changes represent switches between two steady states or if, instead, they result from low-frequency oscillations of the ocean–atmosphere system (18). We discern between internal and forced variability here, because, in four models, such switches in sea ice cover occur in all simulations, including the preindustrial control runs, whereas, in two other models, they only appear after the forcing has passed a certain threshold. In these cases, sea ice must become thin enough for the feedback between open-ocean convection and sea ice to start working. Additionally, the stratification below the sea ice must be able to sustain deep convection. These latter two conditions may be satisfied only after the forcing has changed the climate state sufficiently.

Category II, Type 3, Case g: Abrupt West Tropical Indian Oceanic Bloom. In the RCP projections, a few model studies show that the oceanic primary productivity tends to decrease due to general stratification of the ocean (19). Instead, we found, in IPSL-CM5A-LR, in the RCP8.5 long-term scenario, a very large and abrupt change in integrated primary productivity and many other biogeochemical variables around year 2230, which reverses a few decades later. This type of abrupt change has not been described before. The shift takes place in the western tropical Indian Ocean, close to the coast of Somalia. This event features an increase in equatorial upwelling, which is due to a general increase in oceanic velocity and divergence at the equator associated with enhanced wind stress at the surface linked to changes in monsoon regime. As a consequence of this increased divergence in the equatorial area, the upwelling increases, bringing a large amount of nutrients to the surface that are then advected toward the coast of Somalia, where the bloom is maximal.

The modeled chain of events starts with wind stress changes, first impacting horizontal and vertical ocean currents, and thereafter impacting the biological activity. This chain of events is nonlinear and amplified with each step. Hence, very minor fluctuations of basin-wide surface conditions result, in IPSL-CM5A-LR, in the very abrupt change that we observe at the end of this causal chain. None of the physical variables show distinct abrupt change.

Category III, Type 4, Cases h, i, j, k, and l: Arctic Winter Sea Ice Collapse. Among the forced changes in sea ice, the one of largest geographical extent is the disappearance of all Arctic winter sea ice in the RCP8.5 simulations. We find five cases of such large-scale Arctic winter sea ice collapse. Abrupt winter sea ice loss was previously attributed to a different feedback mechanism (20, 21). The mechanism we propose is a different one (threshold-driven). Once sea ice becomes very thin, the fast warming and the lack of areas

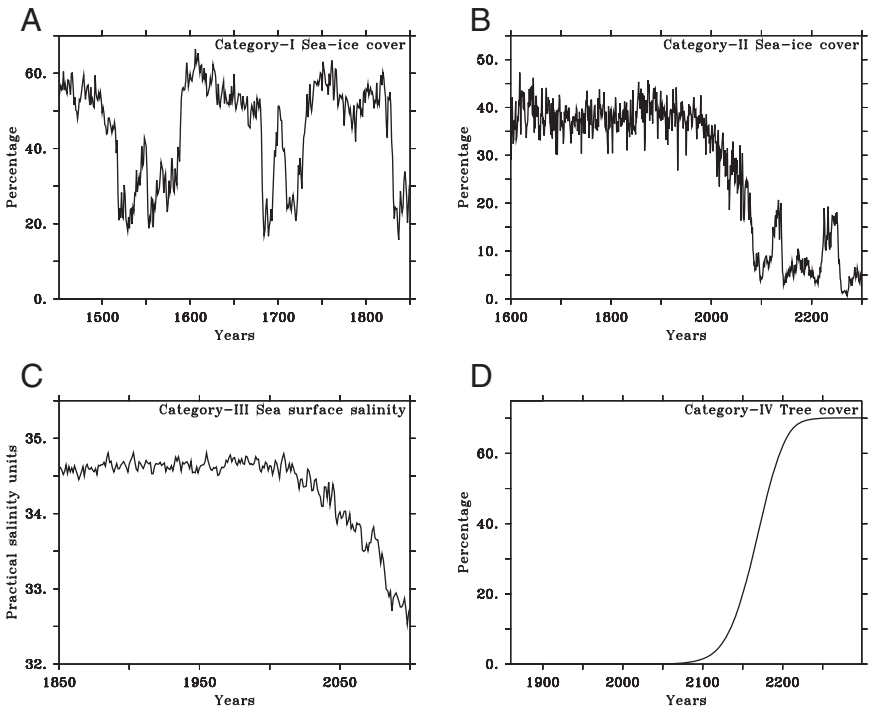

Fig. 2. Examples of different categories of abrupt climate change detected in the CMIP5 database. Evolutions of (*A*) (category I: internally generated switches between two different states, case b in Fig. 1) regional annual mean sea ice cover in the Southern Ocean in the preindustrial control run of bcc-csm1-1-m; (*B*) (category II: a forced transition to switches between two different states, case f in Fig. 1) regional annual mean sea ice cover in the Southern Ocean in the historical and rcp4.5 run of GISS-E2-H; (*C*) (category III: singular rapid abrupt change toward a new state, case t in Fig. 1) SST in the Labrador Sea in the historical and rcp4.5 run of GFDL-ESM2G; and (*D*) (category IV: gradual sequence of abrupt changes toward a new state, case E in Fig. 1) tree cover in the Arctic tundra in the historical and rcp8.5 run of HadGEM2-ES.

with enhanced sea ice thickness can quickly collapse all remaining sea ice in the Arctic. This geometric mechanism does not require radiative feedbacks. Arctic winter sea ice collapse only occurs in RCP8.5 runs that are extended beyond 2100, which represents a small subset of the models. Here, we only retain those cases that meet the abrupt criteria for annual mean values. Further analysis of those cases, however, reveals that the abrupt change in Arctic sea ice cover is usually limited to winter and spring averages. The summer averaged sea ice cover decreases gradually, but a much more accelerated decline appears for winter and spring averages. This implies that for time series of year-to-year changes of a particular season or month, the changes appear faster and more abrupt than when considering annual means. When one considers yearly changes in the March–May average sea ice cover, for instance, the transition appears most abrupt in the MPI-ESM and CSIRO models (approximately a loss of 4–6 million km^2, i.e., a third of the Arctic Ocean, in one decade; see *SI Appendix*, Fig. S1). In the MIROC, HadGEM2-ES, and GFDL models, a collapse also occurs in the winter months. These sea ice collapses occur when the large area of thin ice, which re-forms each winter, suddenly fails to return when temperatures have become sufficiently warm that the freezing point is no longer realized.

Several potential mechanisms to explain abrupt sea ice cover changes have been proposed: the ice albedo feedback (22), the convective cloud feedback (23), and the increased open-water formation efficiency of thin ice (24). In addition, ocean heat transport feedbacks may also play a role (25). The ice albedo feedback and cloud feedback operate with specific timing during the day. Our analysis reveals that the timing of abrupt changes differs among the models. Additional simulations with MPI-ESM confirm that the collapse is not due to albedo or cloud feedbacks in that model. Instead, the simple fact that, at a certain stage, Arctic sea ice thickness becomes thin enough everywhere, combined with the fast forcing and surface melt, is sufficient to explain the rapid area loss: Although it takes decades to melt the present-day thick multiyear sea ice (grown over multiple years), the area extent of sea ice can respond much faster to changes in temperature when sea ice becomes very thin.

Some models have considerable bias in Arctic sea ice thickness in the historical runs, but the mechanism sketched above does not favor too large or too small sea ice in the Arctic at the start of RCP scenario runs. The bias only affects the timing of abrupt change. We also note that this abrupt shift exclusively occurs in the RCP8.5 extended runs after year 2100 and after crossing a temperature threshold that is not reached in RCP2.6 and RCP4.5 scenarios (see *SI Appendix*, Table S1).

Category III, Type 5, Cases m, n, o, and p: Abrupt Regional Sea Ice Loss. In many models, a sudden disappearance of sea ice cover occurs in the RCP projections in parts of the Arctic, Nordic Seas, and Southern Ocean (Fig. 1). We only consider cases in which the annual mean sea ice cover changes abruptly. This type of abrupt change resembles the feedback-driven abrupt shifts in the sea ice edge found in an "aquaplanet" energy balance model (26). It is sometimes associated with changes in ocean deep convection (12). However, the geometric effect of a gradually thinning homogeneous ice cover seems sufficient to explain many of the cases. In CanESM2, sea ice disappears in the Barents Sea in one scenario, and MRI-CGCM3 shows abrupt decreases of sea ice in the Pacific and Atlantic sectors of the Southern Ocean. Based on analysis of model diagnostics, we infer that these events are associated with an increased mixed layer depth, indicating that ocean convection feedbacks likely play a role in these forced changes. Although their magnitude clearly suggests anthropogenic forcing as the main driver, internal climate variability affects the likelihood and timing of the abrupt events. The shifts therefore do not occur in

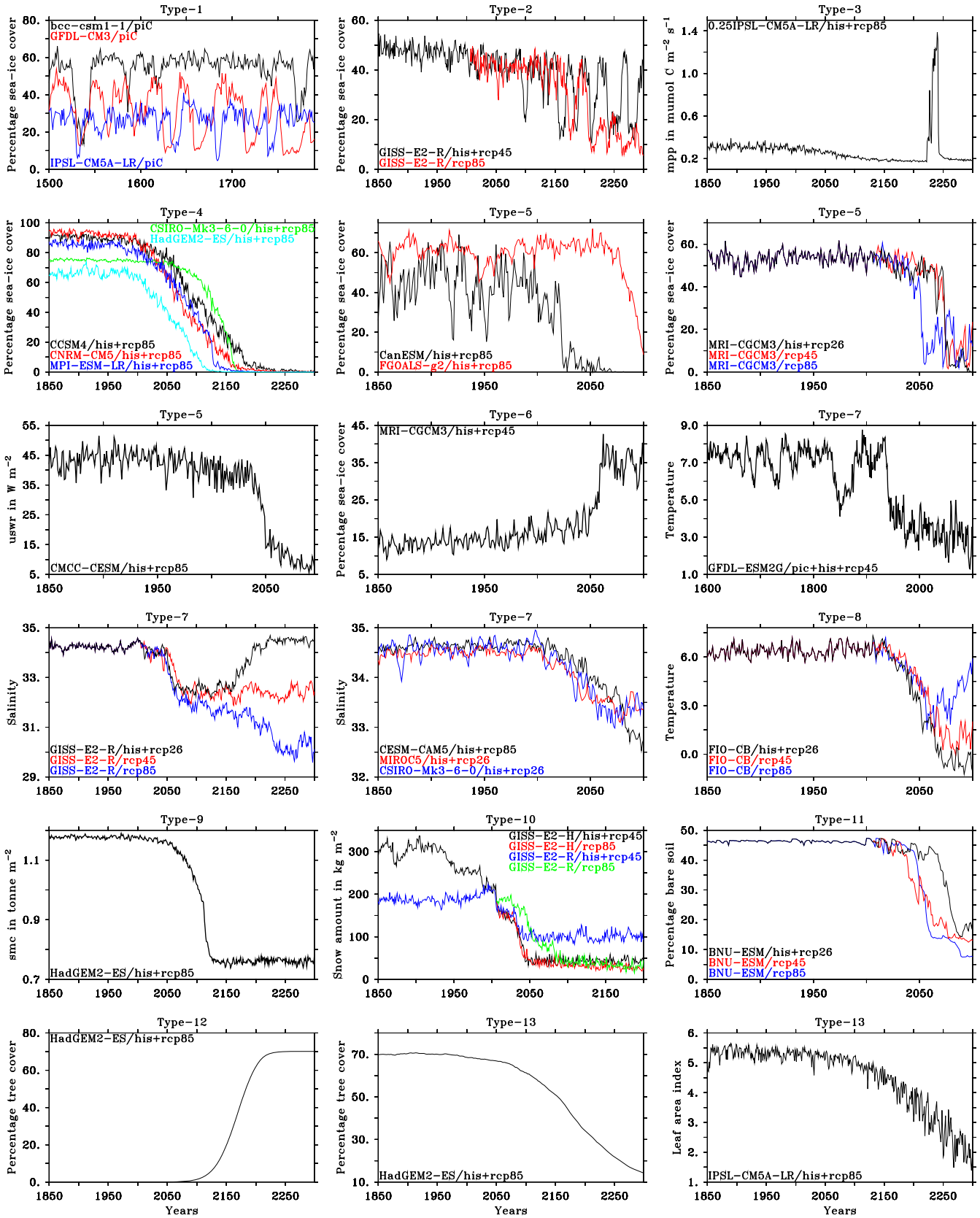

Fig. 3. Time series of all abrupt events not shown in Fig 2. All cases display annual means. Type-2 sic_GISS-E2_R_rcp45 and Type-2 sic-GISS-E2-H_rcp45 are ensemble members r2i1p3; Type-4 sic_CanESM2_rcp85 is ensemble member r5i1p1; Type_10 snw_GISS-E2-R_rcp45 is ensemble member r2i1p2; Type_10 snw_GISS-E2-R_rcp85 is ensemble member r1i1p2; all other types display time series from ensemble member r1i1p1; uswr, upward shortwave radiation; mpp, marine primary production; smc, soil moisture content.

all realizations and scenarios and have no unique global warming threshold beyond which they can be expected. Two models show a local but fast transition from perennial sea ice cover to an annually ice-free ocean: CMCC-CESM in the Barents Sea (case n), and FGOALS-g2 in the Pacific sector of the Southern Ocean (case p). Simultaneously, in those models, the annual mean absorbed shortwave radiation increases by 20 $W \cdot m^{-2}$ and 30 $W \cdot m^{-2}$, indicating the importance of the ice albedo feedback for these local cases.

In most cases, areas of 1 million km^2 or more are suddenly exposed. The models that include an ocean biogeochemistry module show that the events of sea ice loss are generally associated with a sharp increase in productivity, most likely due to light limitation, which could also constitute an additional feedback through its impact on shortwave absorption level in the water column (27). We find no simultaneous shifts in productivity or other physical parameters outside the areas of abrupt sea ice change. Type 5 abrupt shifts also favor the RCP8.5 scenario, but often occur at lower temperature thresholds that are also reached in other less strongly forced scenarios where the same shifts do not occur.

Category III, Type 6, Case q: Abrupt Sea Ice Increase. In MRI-CGCM3, sea ice area increases in the Indian sector of the Southern Ocean for the RCP4.5 simulation. This corroborates the view of sea ice loss as a reversible threshold phenomenon. This type of abrupt change is governed by feedbacks similar to those for types 1 and 2. Also for this type of abrupt change, the shift is most pronounced when one considers sea ice cover averages over winter months only. In general, open-ocean convection locally prevents the formation of sea ice. In the type 6 shift, we observe that, once deep convection stops, a fresh surface layer is formed, enabling the rapid formation of sea ice. In these circumstances, an increase in sea ice cover can be observed, despite the increased global warming.

Category III, Type 7, Cases r, s, t, u, and v: Regional Convection Collapse in the North Atlantic. In the GISS-E2-R, CESM-CAM5, GFDL-ESM2G, MIROC5, and CSIRO-Mk3-6.0 model projections, we observe abrupt changes in the Labrador Sea. Convection in the Labrador Sea suddenly collapses after an increase in stratification in response to warming and freshening of the convective areas and associated decrease in surface density (Fig. 2*C*). In case of a regional convection collapse, the convective salt feedback dominates (28). Large sea surface temperature (SST), sea surface salinity (SSS), and sea ice cover variations are observed in different RCP projections, inducing large regional cooling and a modification in large-scale precipitation patterns. These changes take place during a period of less than 10 y (*SI Appendix*, Fig. S2*A*) and appear in all of the analyzed scenarios. As an example, we examine the GISS-E2-R model for the RCP2.6 scenario. The shift in SST is more than 6 times the SD computed over the historical era, more than 12 times the historical SD for SSS, and more modest (3 times the historical SD) for the Atlantic Meridional Overturning Circulation (AMOC; *SI Appendix*, Fig. S2*A*).

The threshold for abrupt changes in SSS and SST is related to deep ocean convection, which normally occurs during winter in the Labrador Sea, but halts in the model after the threshold is passed. Large changes in vertical stratification occur before and after the abrupt shift (*SI Appendix*, Fig. S2*B*), with a far stronger stratification after the decade 2040–2049 (the density difference between the upper 500 m and the deep ocean increases from 0.15 $kg \cdot m^{-3}$ to more than 0.45 $kg \cdot m^{-3}$). After that, the stratification has become too strong to be broken by winter cooling, which makes deep ocean convection no longer possible. The collapse of convective activity leads to a positive feedback via modifications in ocean circulation, causing less warm and salty Atlantic water entering the Labrador Sea. A summary of the processes involved is sketched in the *SI Appendix*, Fig. S2*C*.

When convection has ceased, a shallow halocline forms in the Labrador Sea, so that mixed layer depth decreases from a few hundred meters to around 10 m. The decrease in thickness of this upper layer then strongly reduces the heat capacity of the active layer in contact with the atmosphere. Thus, sea ice formation becomes more efficient in winter. We observe a strong increase in sea ice cover a few years after the decrease in SST sets in, and SSS changes lead SST changes by around a year (*SI Appendix*, Fig. S2*B*). This change in sea ice cover, in turn, leads to strong cooling of the atmosphere around the Labrador Sea, affecting the global atmospheric circulation. We find, in all models, a cooling in North Atlantic surface air temperature (SAT) by about 2 °C and up to 3–4 °C in GFDL-ESM2G. Such substantial regional changes may influence the large-scale atmospheric circulation, affecting North Atlantic storm tracks (29) or the Intertropical Convergence Zone (30, 31). Indeed, analysis of tropical precipitation shows considerable changes in all five models in response to abrupt changes in ocean convection.

Category III, Type 8, Case w: Collapse of the AMOC. In one instance (FIO-ESM), a gradual weakening of the AMOC, which already set in during the 20th century in the historical simulation, then induces sudden changes in air temperature and sea ice cover (see *SI Appendix*, Fig. S3). These start in the Greenland Sea but affect the whole North Atlantic later on. A collapse of the AMOC is mainly governed by an advective salt feedback (32, 33). We find this event to be associated with indicators of decreasing stability (rising variance and autocorrelation; *SI Appendix*, Fig. S4) (34, 35) for SST but not for the AMOC itself, whereas, in other instances of rapid change investigated, such generic early warning signals are absent. In FIO-ESM, abrupt cooling starts in the Nordic Seas around year 2040 in all four RCP scenarios (*SI Appendix*, Fig. S3*A*). Recovery occurs around year 2050 in the RCP8.5 scenario, whereas, in the other three scenarios, the cooling stabilizes around year 2080. The RCP2.6 scenario features the largest cooling. Inspection of various physical fields and associated time series reveals the following mechanism. As the modeled 20th century progresses, the AMOC starts declining in response to global warming (*SI Appendix*, Fig. S3*B*). Until approximately year 2020, reduced heat transport balances increased radiative forcing and ocean temperatures hardly change. SAT and SST show larger interannual variability between years 1970 and 2020. In this period, the decline of the AMOC accelerates and salinity in the area starts diminishing. After 2020, the increase in radiative forcing is no longer able to compensate for weakened advection of warm water into the area, and SST and SAT start to diminish and the related decrease in salinity accelerates. After year 2040, sea ice starts to form in the area, which was largely ice-free in the period before 2040. Ice albedo feedbacks amplify the cooling, and SST abruptly drops. Between 2040 and 2060, the amplitude of the cooling increases from 3 times the SD to 14 times the SD. SAT follows SST but, normalized with its SD, the signal is weaker, although still 8 SDs.

The AMOC effectively collapses after year 2060. As a result of the AMOC collapse, cooling in the Nordic Seas spreads westward toward other deep water formation areas, like the Labrador Sea. Increase of sea ice in the whole Atlantic sector of the Arctic causes a temperature decrease of more than 4 °C in a 20°-wide latitude band (55°N–75°N), stretching from 60°W to 40°E. Between Iceland and Svalbard, a large region develops that features cooling above 10 °C. South of 40°N and outside the Atlantic, global warming dominates. In the other RCP scenarios, the same mechanism operates, but stronger warming through increased radiative forcing is better able to counteract the cooling associated with the AMOC collapse. Hence the cooling weakens with stronger forcing.

Category III, Type 9, Case A: Arctic Permafrost Collapse. For Arctic tundra, HadGEM2-ES projects a rapid thawing of permafrost; total soil moisture content decreases quickly as the ice in the soil

melts and moisture drains away. This type of abrupt change has not been described before. Shortly after 2100, soil water content declines abruptly, caused by a rapid decrease of ice fraction in the soil. This leaves the soil moisture, now in liquid phase, more susceptible to drought conditions in a changing climate, as it can be evaporated much more easily than frozen water. Due to the substantial latent heat flux involved in the water to ice phase transition, the presence of ice fraction has a stabilizing (dampening) effect on soil temperature and moisture storage. With less ice, however, the rest of the soil potentially warms more quickly, triggering a positive feedback in the soil water storage. To our knowledge, HADGEM2-ES is the only model that accounts explicitly for an ice fraction in the soil. Therefore, other models could not simulate this mechanism.

Category III, Type 10, Cases B and C: Abrupt Tibetan Snow Melt. We observe two cases (models GISS-E2-H and GISS-E2-R) of sudden snow melt on the Tibetan Plateau in more than half of all realizations of RCP4.5 and RCP8.5 runs with those models. Also, this type of abrupt change has not been described before. The most abrupt volume change, from an annual mean of 400 $kg{\cdot}m^{-2}$ down to 50 $kg{\cdot}m^{-2}$ in only 20 y, occurs in a small area at the eastern boundary of the plateau. However, a still relatively rapid decrease of snow amount during the first half of the 21st century occurs over most of the Tibetan Plateau. The snow cover fraction shows a much less pronounced decline than the volume, and is only abrupt in one realization (in the GISS-E2-H model, RCP8.5 scenario). We therefore conclude that the surface albedo feedback via the atmosphere is not the reason for the sudden snowmelt. Instead, the rising temperature drives the system into a regime where the annual mass flux balance becomes negative and snow becomes a seasonal phenomenon. Although the abruptness and magnitude of the change could be an artifact of simplifications in the model and its low resolution, in particular the coarse representation of orography, the general mechanism is well understood, and the region where the largest change is observed is in line with regional climate model simulations (36).

Category III, Type 11, Case D: Abrupt Sahel Vegetation Changes. Vegetation cover in the Sahel region is sensitive to any imposed climate change, or to increased water use efficiency due to the fertilization effect of elevated CO_2 concentrations. We find an abrupt decline in bare soil around year 2050 in the RCP8.5 simulation of BNU-ESM (*SI Appendix*, Fig. S5*A*). Abrupt vegetation cover change is in line with earlier conceptual models (37). However, here it only occurs locally. A transitional spike in the grass fraction follows this shift before a further rapid shift toward enhanced tree cover occurs after year 2060 (*SI Appendix*, Fig. S5*B*). These abrupt changes in vegetation composition in Africa imply Sahel greening and are likely driven by climate change (38) and the ecophysiological effects of raised atmospheric CO_2 concentrations. We note that the responsible drivers and spatial patterns of vegetation cover changes differ among models (39).

Category IV, Type 12, Case E: Transition from Tundra to Boreal Forest. In the extended RCP8.5 simulation (i.e., beyond year 2100) of HadGEM2-ES, vegetation cover in the Arctic above 70°N changes quickly from a mixture of bare soil and shrubs into tree cover after year 2150 (Fig. 2*D*). Although the timescale of forest growth is multidecadal, it is still sufficiently fast to satisfy our formal criteria for abrupt changes. This type of abrupt change is governed by feedbacks similar to those for type 11. The mechanism behind the forest northward expansion is based on increased ability of boreal trees to become more productive and to grow faster under strong warming as simulated by the model. This mechanism is also present in the other models with dynamic vegetation representation in the land surface component, such as MPI-ESM-LR. This is reflected in the IPCC AR5 (figure 6.38 in ref. 40), although the boreal forest expansion in MPI-ESM-LR has stronger interannual variability and therefore is not as abrupt as in HadGEM2-ES. The expansion of boreal forest to the Arctic coast in Eastern Siberia during warmer summer climate in the mid-Holocene is supported by analysis of pollen data (41). There is also a positive feedback between boreal tree cover and temperature due to the snow-masking effect of forest (42), which, however, should ultimately decline in a warmer climate due to shorter snow period.

Category IV, Type 13, Cases F and G: Amazon Forest Dieback. Amazon forest dieback remains one of the iconic potential major changes to the Earth system (43). The most significant terrestrial ecosystem changes we find are indeed for the Amazon forest. The change in vegetation is slower than a decade but still constitutes a major shift to a new regime. In two models, we find the Amazon forest dieback (HadGEM2-ES and IPSL-CM5A-LR) as a consequence of warming or reduced rainfall, impacting photosynthesis (see *SI Appendix*, Fig. S5 *C* and *D*). The complete dieback takes place over more than a few decades. Amazon dieback only occurs in RCP8.5 runs that are extended beyond year 2100. The dieback is particularly notable in one model with dynamic vegetation, HadGEM2-ES. Analysis of the scenario extension to year 2300 highlights how "committed" changes (for a given level of atmospheric greenhouse concentrations reached much earlier—here, year 2100) might not manifest until a longer period after such a particular radiative forcing is realized (44). Anthropogenic land cover changes are absent in the extension of RCP8.5; hence all dynamics from 2100 to 2300 is exclusively due to natural vegetation processes. The tree cover in HadGEM2-ES experiences large changes (*SI Appendix*, Fig. S5*C*). Similar to the tree cover loss observed in earlier versions of the Hadley Centre family of climate models, it is mainly driven by a reduction in precipitation, generating a potential positive feedback between tree cover and precipitation due to reduced moisture recycling (45). The identified shifts only occur in extended RCP8.5 runs and for those two models reaching the highest temperature increase in year 2300.

Discussion

The catalog of abrupt shifts occurring in the CMIP5 multimodel ensemble we present is a first step toward a robust assessment of abrupt change. The catalog is model-based, and climate models have not been evaluated regarding their capability of simulating regional abrupt climate change. Such an attempt could be made if last millennium runs became part of the new CMIP6, although the presence of abrupt volcanic eruptions in the forcing might pose challenges in the evaluation. The number of abrupt shifts identified may seem surprisingly large. In the recent past, it has been claimed that current-generation climate models are largely incapable of simulating historic abrupt events (46), as the models are tuned for being too stable. We find that many types of abrupt change occur in simulations with the present-generation climate models, especially in climate change scenarios.

A striking feature is that the majority of abrupt transitions occur in the ocean–sea ice system, implying that this Earth system component is more prone to abrupt change than other components. This finding is in line with studies that have highlighted the important role of sea ice for abrupt climate change in Earth's history (47, 48). Sea ice is a plausible source of abrupt change for the following reasons: It can respond on a very short time scale (little inertia); it has very strong feedbacks, notably the ice albedo feedback; and the freezing point is a strong "binary" natural threshold (49).

Abrupt changes in terrestrial ecosystems and soils are not as pronounced in CMIP5 simulations. This could be explained in several ways. Few models calculate vegetation dynamics (i.e., changes in spatial distribution of vegetation cover in response to climate and CO_2 change), and thus the CMIP5 database only samples a subset of potential behavior. Furthermore, the dynamics of woody vegetation, such as trees or shrubs, respond

relatively slowly (decades rather than years). In addition, local biophysical feedbacks between land and atmosphere may be relatively weak compared with feedbacks involving sea ice cover and ocean convection. Lastly, heterogeneity of the land surface leads to smoothing of vegetation changes (50). In general we find no evidence of ecosystem collapses, except the case of Amazon dieback. However, ecosystem variables were often not available in the output.

Abrupt shifts due to internal variability (also occurring in preindustrial runs) are present in 11% of the models [3.9 out of 37 accounting for the fraction in each model ensemble (*SI Appendix, SI Methods*)]. We find three cases of sequences of reversing switches after a certain temperature threshold is passed in the RCP scenarios (category II). In one case, a single reversing switch occurs. All other cases we identify are nonreversing shifts that occur in historical plus RCP scenario simulations. These forced shifts occur after passing a temperature threshold. Eighteen out of 37 forced abrupt shifts occur in simulations for global warming levels below 2° (Fig. 4), a threshold often proposed as a potentially safe upper bound on global warming (6). The frequency of occurrence, that is, the fraction of abrupt events per model run, is 33% for the RCP scenarios and 53% for the RCP8.5 scenario (*Methods* and *SI Appendix*, Table S1). This result suggests that it is likely that the Earth system will experience sharp regional transitions at moderate warming, although the prediction of any particular event has a very high uncertainty.

When ranking the abrupt shifts against temperature (Fig. 5), a minimum amount of shifts occurs between 3° and 5° temperature increase, although this minimum is not statistically significant. It arises because many ocean and sea ice changes are related to shifts in open-ocean convection, which occur for relatively moderate temperature increases, whereas shifts in the terrestrial system and Arctic winter sea ice occur for much larger temperature increases. The RCP8.5 scenario shows more shifts than the RCP4.5 scenario, even in the range of temperature increases they have in common, suggesting that not only amplitude but also speed of temperature increase is destabilizing. Another caveat in ranking abrupt shifts against temperature increase is that small temperature increases are associated with more simulation years than larger temperature increases. Due to differences in the scenario selection for each model, and differences in climate sensitivity between models, the temperature space in CMIP5 is not well sampled, preventing further statistical analysis of the relation between abrupt events and global temperature change. No

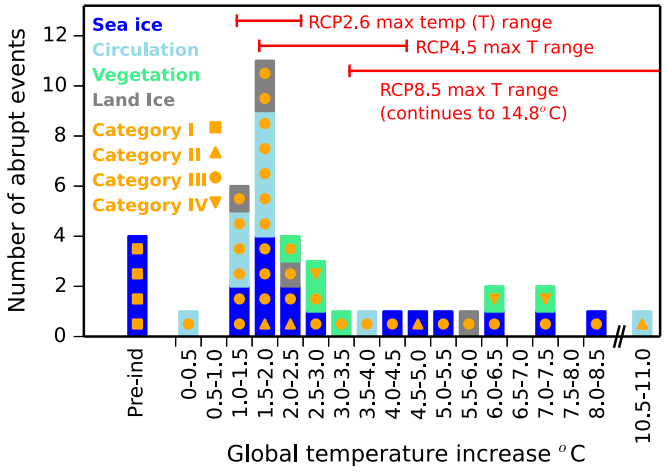

Fig. 4. Abrupt shifts as a function of global temperature increase. Shown are the number of abrupt climate changes occurring in the CMIP5 database for different intervals of warming relative to the preindustrial climate.

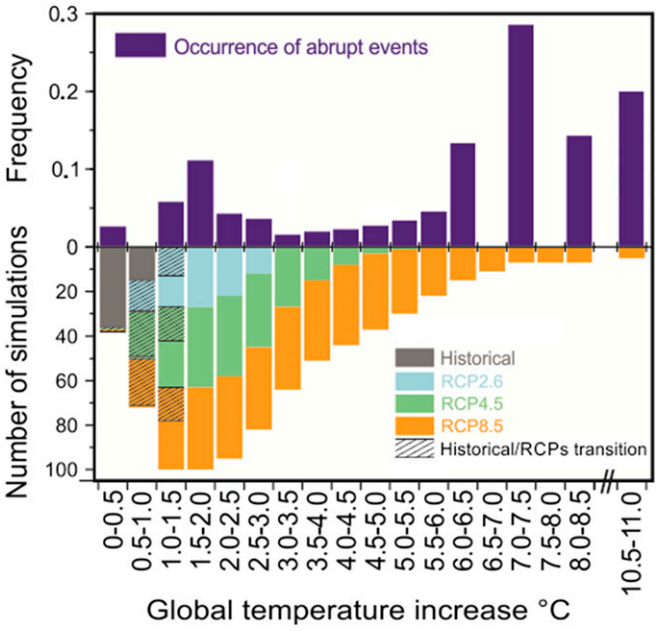

Fig. 5. The frequency of occurrence of forced abrupt shifts as a function of global temperature increase. This number depends on the width of the temperature interval. Nevertheless, its qualitative shape gives an indication of how forced abrupt changes are divided over the range of temperature increases relative to the preindustrial area as simulated by the CMIP5 models. The frequency of occurrence is displayed per 0.5° temperature interval; see also *Methods*. Forced abrupt shifts occur only once in a particular scenario.

type of abrupt shifts occurs in all models. Many of them occur by chance; that is, they depend sensitively on details in the simulated climate state, including natural variability. Some depend on model (bio)physics, (oversimplified) parameterizations, or thresholds not being reached in other model simulations.

Most abrupt shifts found in our analysis have been previously identified and possible mechanisms proposed, although often using simplified models (4). Exceptions include abrupt change in the marine productivity (case g) and permafrost thaw and snow melt (cases A, B, and C). Permafrost carbon release (51) and methane hydrates release (52) were not expected in CMIP5 simulations, because of missing biogeochemical components in those models capable of simulating such changes. Proposed abrupt changes in monsoon circulation (53) and in long-term droughts (54) were not found, possibly due to limitations of our method focusing on annual mean data. Boreal forest dieback at the southern forest border (2) was not found; however, we identified an example of boreal forest expansion to tundra (case E) expected in a warmer climate. This abrupt expansion is linked to the permafrost collapse in high-latitude regions, as its thaw allows shrubs and trees to develop roots in deeper soil layers. Although, in the CMIP5 experiments, permafrost and vegetation were not interacting, this is an example of a possible cascade of abrupt changes as a shift in one climate subsystem (cryosphere) subsequently causes abrupt changes in another domain (vegetation).

The character, timing, and location of abrupt events we detect are model-specific, illustrating the uncertainty associated with predicting particular events. Sometimes, simpler or older non-CMIP5 models suggest tipping points that disappear in more-complex versions (55). Alternatively, CMIP5 models could underrepresent the likelihood of abrupt shifts. For instance, there is some reluctance to upload simulations to the CMIP5 database, that contain large abrupt changes [e.g., a collapse of the AMOC (56)], representing a behavior not observed in the

(historical) record. Also, models that produce shifts that at first sight seem implausible or unphysical are often retuned. Both practices could bias the CMIP5 database toward containing more-stable configurations (57). An additional concern is that the present generation of climate models still does not account for several mechanisms that could potentially give rise to abrupt change. This includes ice sheet collapse, permafrost carbon decomposition, and methane hydrates release. An improved CMIP6 would contain at least a few models that have made a start to incorporate these processes. Also, it would contain more multimember experiments to better understand and quantify the frequency of abrupt events, allowing for more robust statistics.

Methods

Search Criteria. To systematically scan all available CMIP5 data for abrupt events, we calculated three different quantities from the annual mean time series at each grid cell: (*i*) the mean difference averaged over 10 y between the end and beginning of a simulation; (*ii*) the SD of the 10-y running mean of the time series; and (iii) the maximum absolute change occurring within 10 y in the 10-y running mean of the time series.

For every model simulation and variable under investigation, we constructed global maps of these three quantities and identified potential areas of abrupt change by eye as regional maxima on the maps. Different phenomena cause different signals on the maps. Fluctuations between two regimes do not necessarily influence quantity 1, but have a signal in quantities 2 and 3. Singular collapses can be seen in all three quantities; very large but gradual changes are covered by quantities 1 and 2, but not necessarily by quantity 3.

The search criteria are sensitive to abrupt change, demonstrated by using a Gaussian white noise process as an example, as evidenced in *SI Appendix*, Fig. S6. The process has an SD of unity, and its mean is linearly increasing in time, apart from one abrupt step change. For different sizes of this step change, we generated 100 realizations of time series and obtained a sampling distribution for each indicator of abrupt change (difference, SD, and maximum absolute change). The indicator increases with increasing step size and becomes more robust when the step change emerges from the noise.

We also compared our results to the properties of the preindustrial control simulations (piControl) (the red time series in *SI Appendix*, Fig. S6*A*). This allowed us to distinguish prominent features of internal variability from forced transitions and to detect cases where an indicator of abrupt change is not larger in a particular region than elsewhere, but is much larger than in piControl. The search criteria were also applied to the piControl runs to search for unforced abrupt events that are part of the system's natural variability.

The emphasis of our study is on geographical (i.e., latitude and longitude) 2D, annual mean fields. These are, for the ocean: sea ice cover, SST, SSS, and AMOC; for the atmosphere: 2-m-height temperature, sea level pressure, and precipitation; for vegetation: tree fraction, grass fraction, and leaf area index; for the soil: soil moisture (not routinely) and gross primary production; for radiation: surface albedo (not routinely) and upward and downward solar radiation; and for ocean biogeochemistry: surface CO_2 partial pressure, surface sea air CO_2 partial pressure difference, carbon sinking flux of particulate matter, total downward CO_2 flux, and primary productivity.

Where our search criteria suggested locations of major change, we constructed time series for area averages and visually inspected these for potentially abrupt shifts standing out from the internal variability.

Classification Criteria. The cases that emerged from the search procedure as potentially interesting were subsequently scrutinized more closely with respect to three quantitative criteria. Our next step consisted of ensuring that, for forced abrupt shifts (categories II, III, and IV), the maximum 10-y change in an RCP scenario was exceeding 4 SDs in the annual mean time series of the preindustrial control runs. All category II and III shifts, as well as the slower changes of category IV, are required to fulfill this criterion. This first classification criterion ensures that the magnitude of shifts we identified is very large relative to preindustrial variability.

As a second criterion for classification, we applied two nonparametric tests to verify whether the underlying probability density function of the time series was either multimodal (sign of multiple regimes) or asymmetric (sign of large departure from the main regime). This is to verify that the large step exceeding 4σ is not an outlier from a normal background distribution, but is instead a consequence of changing time characteristics. This second criterion is only applied for forced shifts that obey the 4σ criterion and serves as an extra constraint for the shifts to be classified as abrupt changes. For naturally occurring, large, reversing shifts sometimes occurring in the preindustrial runs, this second criterion is the only classification criterion that we applied after preselection by the previous search criteria. We achieved these classifications by either the Dip test (58) or a Symmetry test based on the nonparametric skewness (59) (*SI Appendix, SI Methods*).

ACKNOWLEDGMENTS. We thank Vasilis Dakos for making the early warning signals toolbox available and two anonymous referees for their supportive comments. This work was funded by the European Commission's 7th Framework Programme, under Grant Agreement 282672, EMBRACE project.

1. Intergovernmental Panel on Climate Change (2013) *Climate Change 2013: The Physical Science Basis*, eds Stocker TF, et al. (Cambridge Univ Press, New York).
2. Lenton TM, et al. (2008) Tipping elements in the Earth's climate system. *Proc Natl Acad Sci USA* 105(6):1786–1793.
3. Levermann A, et al. (2012) Potential climatic transitions with profound impact on Europe—Review of the current state of six 'tipping elements of the climate system.' *Clim Change* 110(3):845–878.
4. Collins M, et al. (2013) Long-term climate change: Projections, commitments and irreversibility. *Climate Change 2013: The Physical Science Basis* (Cambridge Univ Press, New York), pp 1029–1076.
5. Rockström J, et al. (2009) A safe operating space for humanity. *Nature* 461(7263): 472–475.
6. Jaeger CC, Jaeger J (2011) Three views on two degrees. *Reg Environ Change* 11 (Suppl 1):15–26.
7. Knutti R, Hegerl GC (2008) The equilibrium sensitivity of the Earth's temperature to radiation changes. *Nat Geosci* 1:735–743.
8. Taylor KE, Stouffer RJ, Meehl GA (2012) An overview of CMIP5 and the experiment design. *Bull Am Meteorol Soc* 93(4):485–498.
9. Meinshausen M, et al. (2011) The RCP greenhouse gas concentrations and their extensions from 1765 to 2300. *Clim Change* 109(1):213–241.
10. Rahmstorf S (2001) Abrupt Climate Change. *Encyclopedia of Ocean Sciences*, eds Steele J, Thorpe S, Turekian K (Academic, London), pp 1–6.
11. National Research Council (2002) *Abrupt Climate Change: Inevitable Surprises* (Natl Acad Press, Washington, DC).
12. Lenderink G, Haarsma RJ (1996) Modeling convective transitions in the presence of sea ice. *J Phys Oceanogr* 26(8):1448–1467.
13. Heuzé C, Heywood KJ, Stevens DP, Ridley JK (2013) Southern Ocean bottom water characteristics in CMIP5 models. *Geophys Res Lett* 40(7):1409–1414.
14. Gordon AL (2014) Oceanography: Southern Ocean polynya. *Nat Clim Change* 4:249–250.
15. de Lavergne C, Palter JB, Galbraith ED, Bernardello R, Marinov I (2014) Cessation of deep convection in the open Southern Ocean under anthropogenic climate change. *Nat Clim Change* 4:278–282.
16. Marshall J, Schott F (1999) Open-ocean convection: Observations, theory and models. *Rev Geophys* 37(1):1–64.
17. Carsey FD (1980) Microwave observation of the Weddell Polynya. *Mon Weather Rev* 108(12):2032–2044.
18. Martin T, Park W, Latif M (2012) Multi-centennial variability controlled by Southern Ocean convection in the Kiel Climate Model. *Clim Dyn* 40(7-8):2005–2022.
19. Bopp L, Aumont O, Cadule P, Alvain S, Gehlen M (2005) Response of diatoms distribution to global warming and potential implications: A global model study. *Geophys Res Lett* 32(19):L19606.
20. Eisenman I, Wettlaufer JS (2009) Nonlinear threshold behavior during the loss of Arctic sea ice. *Proc Natl Acad Sci USA* 106(1):28–32.
21. Eisenman I (2012) Factors controlling the bifurcation structure of sea ice retreat. *J Geophys Res* 117(D1):D01111.
22. Winton M (2006) Does the Arctic sea ice have a tipping point? *Geophys Res Lett* 33(23):L23504.
23. Abbot DS, Tziperman E (2008) Sea ice, high-latitude convection, and equable climates. *Geophys Res Lett* 35(3):L03702.
24. Notz D (2009) The future of ice sheets and sea ice: between reversible retreat and unstoppable loss. *Proc Natl Acad Sci USA* 106(49):20590–20595.
25. Abbot DS, Walker CC, Tziperman E (2009) Can a convective cloud feedback help to eliminate winter sea ice at high CO_2 concentrations? *J Clim* 22(21):5719–5731.
26. Rose BEJ, Marshall J (2009) Ocean heat transport, sea ice, and multiple climate states: Insights from energy balance models. *J Atmos Sci* 66(9):2828–2843.
27. Lengaigne M, et al. (2009) Biophysical feedbacks in the Arctic Ocean using an Earth system model. *Geophys Res Lett* 36(21):L21602.
28. Rahmstorf S (1995) Multiple convective patterns and thermohaline flow in an idealized OGCM. *J Clim* 8(12):3028–3039.
29. Woollings T, Gregory JM, Pinto JG, Reyers M, Brayshaw DJ (2012) Response of the North Atlantic storm track to climate change shaped by ocean–atmosphere coupling. *Nat Geosci* 5:313–317.
30. Swingedouw D, et al. (2009) Impact of freshwater release in the North Atlantic under different climate conditions in an OAGCM. *J Clim* 22(23):6377–6403.
31. Drijfhout SS (2010) The atmospheric response to a THC collapse: Scaling relations for the Hadley circulation and the nonlinear response in a coupled climate model. *J Clim* 23(3):757–774.
32. Stommel H (1961) Thermohaline convection with two stable regimes of flow. *Tellus* 13(2):224–230.

33. Marotzke J, Welander P, Willebrand J (1988) Instability and multiple steady states in a meridional-plane model of the thermohaline circulation. *Tellus, A* 40(2):162–172.
34. Scheffer M, et al. (2009) Early-warning signals for critical transitions. *Nature* 461(7260):53–59.
35. Scheffer M, et al. (2012) Anticipating critical transitions. *Science* 338(6105):344–348.
36. Shi Y, Gao X, Wu J, Giorgi F (2011) Changes in snow cover over China in the 21st century as simulated by a high resolution regional climate model. *Environ Res Lett* 6: 045401.
37. Brovkin V, Claussen M, Petoukhov V, Ganapolski A (1998) On the stability of the atmosphere-vegetation system in the Sahara/Sahel region. *J Geophys Res* 103(D24):31613–31624.
38. Claussen M, et al. (2003) Climate change in Northern Africa: The past is not the future. *Clim Change* 57(1-2):99–118.
39. Bathiany S, Claussen M, Brovkin V (2014) CO_2-induced Sahel greening in CMIP5 Earth System Models. *J Clim* 27(19):7163–7184.
40. Ciais P, et al. (2013) Carbon and other biogeochemical cycles. *Climate Change 2013: The Physical Science Basis* (Cambridge Univ Press, New York), pp 465–570.
41. Prentice IC, Jolly D (2000) Mid-Holocene and glacial-maximum vegetation geography of the northern continents and Africa. *J Biogeogr* 27(3):507–519.
42. Brovkin V, et al. (2003) Stability analysis of the climate-vegetation system in the northern high latitudes. *Clim Change* 57(1-2):119–138.
43. Cox PM, Betts RA, Jones CD, Spall SA, Totterdell IJ (2000) Acceleration of global warming due to carbon-cycle feedbacks in a coupled climate model. *Nature* 408(6809):184–187.
44. Jones C, Lowe J, Liddicoat S, Betts R (2009) Committed terrestrial ecosystem changes due to climate change. *Nat Geosci* 2:484–487.
45. Betts RA, et al. (2004) The role of ecosystem-atmosphere interactions in simulated Amazonian precipitation decrease and forest dieback under global climate warming. *Theor Appl Climatol* 78(1-3):157–175.
46. Clement AC, Peterson LC (2008) Mechanisms of abrupt climate change of the last glacial period. *Rev Geophys* 46(4):1–39.
47. Dansgaard W, White JCW, Johnsen SJ (1989) The abrupt termination of the Younger Dryas climate event. *Nature* 339(6225):532–534.
48. Li C, Battisti DS, Schrag DP, Tziperman E (2005) Abrupt climate shifts in Greenland due to displacements of the sea ice edge. *Geophys Res Lett* 32(19):L19702.
49. Gildor H, Tziperman E (2003) Sea-ice switches and abrupt climate change. *Philos Trans A Math Phys Eng Sci* 361(1810):1935–1942, and discussion (2003) 361(1810):1942–1944.
50. Brook BW, Ellis EC, Perring MP, Mackay AW, Blomqvist L (2013) Does the terrestrial biosphere have planetary tipping points? *Trends Ecol Evol* 28(7):396–401.
51. Koven CD, et al. (2011) Permafrost carbon-climate feedbacks accelerate global warming. *Proc Natl Acad Sci USA* 108(36):14769–14774.
52. Archer D, Buffett B, Brovkin V (2009) Ocean methane hydrates as a slow tipping point in the global carbon cycle. *Proc Natl Acad Sci USA* 106(49):20596–20601.
53. Levermann A, Schewe J, Petoukhov V, Held H (2009) Basic mechanism for abrupt monsoon transitions. *Proc Natl Acad Sci USA* 106(49):20572–20577.
54. Held IM, Soden BJ (2006) Robust responses of the hydrological cycle to global warming. *J Clim* 19(21):5686–5699.
55. Yin J, Stouffer RJ (2007) Comparison of the stability of the Atlantic thermohaline circulation in two coupled atmosphere-ocean general circulation models. *J Clim* 20(17):4293–4315.
56. Drijfhout S, Gleeson E, Dijkstra HA, Livina V (2013) Spontaneous abrupt climate change due to an atmospheric blocking–sea-ice–ocean feedback in an unforced climate model simulation. *Proc Natl Acad Sci USA* 110(49):19713–19718.
57. Valdes P (2011) Built for stability. *Nat Geosci* 4:414–416.
58. Hartigan JA, Hartigan PM (1985) The Dip test of unimodality. *Ann Stat* 13(1):70–84.
59. Mira A (1999) Distribution-free test for symmetry based on Bonferroni's measure. *J Appl Stat* 26(8):959–972.